Available online at www.sciencedirect.com
ScienceDirect
International Journal of Heat and Fluid Flow 28 (2007) 963–977
International Journal of HEAT AND FLUID FLOW
www.elsevier.com/locate/ijhff

Airflow patterns in a slot-ventilated enclosure partially loaded with empty slotted boxes

Mitoubkieta Tapsoba [a], Jean Moureh [a,*], Denis Flick [b,1]

[a] UMR Génie Industriel Alimentaire (Cemagref/ENSIA/INAPG/INRA), Refrigeration Process Engineering Research Unit, Cemagref, BP. 44, 92163 Antony Cedex, France
[b] UMR Génie Industriel Alimentaire (Cemagref/ENSIA/INAPG/INRA), 16, rue Claude Bernard, 75231 Paris Cedex 05, France

Received 29 July 2005; received in revised form 5 January 2006; accepted 12 March 2007
Available online 4 June 2007

Abstract

A reduced-scale model and CFD predictions were used to investigate experimentally and numerically the airflow patterns within a ceiling-slot ventilated enclosure loaded by slotted boxes. The experiments were carried out with a laser Doppler anemometer. This paper concerns the air velocity characteristics within the jet and outside the boxes. Results make it possible to highlight the confinement effect due to enclosure and the influence of load porosity on the jet penetration, its development and hence the heterogeneity of ventilation within the enclosure. The numerical predictions obtained with the computational fluid dynamics Fluent package using the RSM turbulence model show rather good agreement with experimental data.

Keywords: Enclosure; Slotted obstacles; Ceiling jet; Airflow pattern; Computational fluid dynamics

1. Introduction

The aim was to characterize experimentally and numerically the airflow patterns within a long ceiling-slot ventilated enclosure loaded by slotted boxes. The results concerned air velocity, turbulence and ventilation rate in the load. The analysis focused on the influence of a permeable load (empty slotted boxes) on jet penetration comparing the results to those obtained by Moureh et al. (2002) for an empty enclosure and Menia (2001) for an enclosure loaded with impermeable boxes.

2. Bibliography analysis

Slot-ventilated enclosures are extensively used in many engineering applications such as buildings (Awbi, 1989; Karimipanah, 1999), animal houses (Bjerg et al., 2002; Gebremedhin and Wu, 2003) and engineering facilities for food transport and storage (Sharp and Irving, 1991; Yu and Hoff, 1999; Moureh and Flick, 2005). A major concern is to provide a better control of ambience parameters such as temperature, humidity and contaminants, which affect the microenvironment around persons, animals, plants or food. The level and the uniformity of these parameters are highly governed by behaviour of airflow patterns and the homogeneity of the ventilation through the load.

Within the slot-ventilated enclosure, the turbulent flow is obtained by injection of a jet at a high velocity parallel and near to the ceiling. Due to the adherence of the jet on this boundary by the Coanda effect, this design should allow the confined jet to expand while following the room

* Corresponding author. Tel.: +33 1 40 96 60 88; fax: +33 1 40 96 62 49.
E-mail addresses: serge.tapsoba@cemagref.fr (M. Tapsoba), jean.moureh@cemagref.fr (J. Moureh), flick@inapg.inra.fr (D. Flick).
[1] Tel.: +33 1 44 08 72 39; fax: +33 1 44 08 16 66.

0142-727X/$ - see front matter © 2007 Elsevier Inc. All rights reserved.
doi:10.1016/j.ijheatfluidflow.2007.03.008

Nomenclature

$C_\varepsilon C_{\varepsilon 2} C_\mu$	empirical turbulence model constants
C	pressure drop coefficient
D	ceiling-inlet distance (m)
D_H	hydraulic diameter (m)
e	interstice distance between boxes (m)
H	enclosure height (m)
h	inlet height (m)
I	velocity standard deviation $\frac{\sqrt{u_i^2}}{U}$
k	turbulent kinetic energy $\frac{1}{2}u_i^2$ ($m^2\ s^{-2}$)
K_p	porous media permeability (m^2)
L	enclosure length (m)
L_p	jet penetration distance (m)
P	pressure (Pa)
Re	Reynolds number
u	velocity fluctuation ($m\ s^{-1}$)
U^+	adimensional velocity $U/\sqrt{\tau_w/\rho}$
U	time-averaged velocity ($m\ s^{-1}$)
U_τ	shear velocity $\sqrt{\tau_w/\rho}$ ($m\ s^{-1}$)
W	enclosure width (m)
x, y, z	space coordinates (m)
y^+	dimensionless wall distance $y\frac{U_\tau}{\nu}$

Greek symbols

α, β, γ	empirical constants
ε	turbulent dissipation rate ($m^2\ s^{-3}$)
δ_{ij}	Kronecker symbol
μ	laminar dynamic viscosity (Pa s)
μ_t	turbulent viscosity (Pa s)
ν	kinematic viscosity ($m^2\ s^{-1}$)
κ	Von Karman constant
ρ	density ($kg\ m^{-3}$)
$\sigma_k, \sigma_\varepsilon$	empirical turbulence model constants.
τ_w	wall shear stress (Pa)

Subscript

$\perp$	normal
0	relative to inlet boundary condition
i, j, k	relative to coordinate system
ref	reference value
t	turbulent
vis	viscous
x, y, z	relative to coordinate system
ε	relative to turbulent dissipation rate

wall surfaces and hence to provide a high degree of ventilation within the whole enclosure.

2.1. Empty enclosures

Numerous studies have been carried out to characterize airflow patterns in empty slot-ventilated enclosure as a function of inlet and outlet locations and dimensions, room size, and inlet jet momentum: Yu and Hoff (1999), Karimipanah (1999), Adre and Albright (1994), Zhang et al. (2000), Awbi (1989), Nielsen et al. (1978), Davidson (1989), Hoff et al. (1992), Choi et al. (1990) and Nady et al. (1995). This paper focuses on the case where inlet and outlet sections are located on the same side. In such a configuration, an adverse pressure gradient arises when the jet approaches the opposite wall (Karimipanah, 1999; Moureh and Flick, 2005; Moureh et al., 2002; Risso and Fabre, 1997). This configuration also causes strong interactions in the transverse direction between the two opposing streams supplying inlet and outlet sections where a high rate of shear stresses occurred in their outer layers. These aerodynamic effects could affect the stability and the maintaining of the wall-jet on the ceiling, limit its development and decrease its penetration into the confined enclosure. This leads to uneven air distribution (Moureh et al., 2002; Lindqvist, 1998) implying high velocities between inlet and outlet sections located in the front side and lower velocities on the rear opposite side.

To express airflow ventilation performance quantitatively into the enclosure, Adre and Albright (1994) define wall-jet penetration (L_p) as the distance from the inlet where the jet velocity vanishes. They found that this distance was approximately 0.64 times the length of the enclosure ($L/H = 2$). In an analogous configuration, Yu and Hoff (1999) used airflow visualization to quantify air-jet penetration and found that this distance was approximately 0.84 times the length of the enclosure. Karimipanah (1999) stated that the wall jet begins to be affected by the opposite wall at $0.7L$ where the pressure starts to increase ($L/H = 2/3;\ 1;\ 4/3;\ 2$). All these studies confirm that the penetration distance remains independent of Re for turbulent jet flow.

Concerning airflow patterns only in short enclosures ($L/H \leqslant 2$), Yu et al. (2003) found that that the jet arrived at the opposite wall, was deflected at the corner and was constrained to follow the room surfaces. It results a fully rotary flow with one recirculating bubble entirely occupying the confined space. Similar results concerning airflow patterns were obtained by Adre and Albright (1994), Timmons et al. (1980), Yu and Hoff (1999) and Davidson (1989). These authors agree that when the inlet Re of airflow exceeds a threshold value, airflow patterns remain independent of increased inlet Re. Obviously, in short configurations, the jet has enough kinetic energy to face the adverse pressure forces only when the Re number is above a threshold value.

Yu et al. (2003) showed that along the ceiling the centerline velocity decreased in two different steps. In the first one, which corresponds to the zone following core region ($10h < z < 100h$), the centerline velocity followed the char-

acteristic decay of plane unconstrained wall jet described as:

$$U_{max}/U_0 = C_w\sqrt{\frac{h}{z}} \quad (1)$$

where C_w is referred to be the inlet constant.

Beyond $100h$, when the jet approaches the opposite wall, the wall-jet collapsed rapidly: velocity values becomes low but still remain positive. This clearly indicated that the wall jet remained attached to the ceiling.

Concerning the longest enclosures, with high L/H ratios, experimental data given by Moureh and Flick (2003) for $L/H > 5$, confirmed that the adverse pressure gradient strongly affected the stability of the wall-jet and caused its separation on the ceiling at $z/L = 0.7$. As a result, two main opposite recirculating bubbles are observed in the symmetry plane on both sides of the separation point. A similar result was obtained by Risso and Fabre (1997) in a fundamental and experimental analysis of the turbulence concerning an axisymmetrical jet within a closed and long tube ($L/d \geqslant 6.7$), where d is the tube diameter. The authors pointed out the presence of an adverse pressure gradient generated by the lateral flow confinement, which in turn makes the mean velocity to drop faster along the jet axis. Nevertheless, instead of approaching zero asymptotically, the mean velocity cancels near $z = 3.6d$ even when the length tube is varied ($L/d = 6.7$, 7.7, and 9.7).

2.2. Loaded enclosures

The influence of slotted obstacles in the enclosure on the flow patterns is one of the main concerns of the present investigation. Obstacles affect the airflow by surface stresses, porous infiltration, deviations and reattachment and also turbulence generation. They may create secondary recirculating flows, including stagnant zones and induce high velocities elsewhere.

When the load is structured as a regular package of impermeable boxes (Wang and Touber, 1988; Moureh et al., 2002; Menia, 2001) the general behaviour of flow can be modelled as a hydraulic pipe network (one pipe for each channel between pallets). However this simplified and global approach is not locally accurate and is not suitable in the slotted boxes case where flow is more complex.

Concerning the influence of obstacles on airflow patterns, Moureh and Flick (2003) and Moureh et al. (2002), pointed out that the compactness of the load increases the confinement effect, which in turn causes a more pronounced adverse pressure gradient. This limits the jet development and strongly affects its stability. As a consequence, the separation point is located at ($z/L = 40\%$) in the case of the loaded configuration instead of ($z/L = 75\%$) for the same unloaded configuration. Choi et al. (1990) presented a numerical investigation of the effects of a rectangular obstacle on airflow in a slot-ventilated enclosure. While the incoming jet deflects upward and attaches to the top wall in the space without any obstacles, the jet deflects downward and attaches to the top of the obstacle where there is one. The author explained this effect by a dominating adverse pressure gradient created by the obstacle. However, these predictions need to be validated experimentally.

All these studies pointed to the existence of an uneven distribution of the airflow, implying a high degree of ventilation heterogeneity within the load. However the lack of accurate experimental data does not make it possible to analyse the mechanisms governing the airflow distribution and ventilation efficiency inside bulk storage. These studies also raised the difficulty of experimental investigation and showed the value of CFD prediction to complete the experimental approach.

2.3. CFD numerical modelling

The turbulent wall jet (even with an isothermal co-flowing or stationary external stream) is known to be a difficult flow to predict (Craft and Launder, 2001). An undeniable difficulty arises through confinement effect and through the presence of slotted boxes. This leads to strong interactions between airflow, surrounding walls, slotted boxes and adverse pressure gradient. The resulting flow is complicated since it is often the combination of free turbulent shear flows, near-wall effect, recirculation areas (including high streamline curvature and probably local separation). It also comprises dynamic interactions between airflows developed outside and inside the slotted boxes. The internal airflow in slotted boxes could be viewed as secondary flow generated by pressure gradient and lateral exchanges through slotted box walls with the external main flow.

In a fundamental analysis concerning confined airflows, Risso and Fabre (1997) pointed out that turbulence is close to Gaussianity only in the inlet region where turbulence is controlled by the mean velocity gradient and production terms. On the contrary, in the confined diffusive region, located downstream from the separation of the jet, the velocity field is non-Gaussian and the flow is highly intermittent. In this region, flow is governed by turbulence diffusivity and triple correlations play an important role. Another difficulty is the anisotropy of the largest scales which are a consequence of the flow confinement. According to these aspects, the authors Risso and Fabre (1997) considered that adjusting the constants of the k–ε model could lead to contradictory results.

Numerous studies use the standard k–ε model described by Launder and Spalding (1974) to predict airflow patterns in enclosures since it is easy to program and has broad applicability: Lamers and Van de Velde (1989), Awbi (1989), Wang and Touber (1988), Choi et al. (1988), Choi et al. (1990), Karimipanah and Sandberg (1994), Bushmann et al. (1994), Mariotti et al. (1995), El Hadidi (1998), Hoang et al. (2000) and Bjerg et al. (2002). However, in the major cases the validation of the turbulence model lacks comparisons with accurate experimental data concerning airflow patterns, especially in 3D cases.

According to the complexity of the indoor flows underlined above, different authors (Wilcox, 1994; Menter, 1997; Nallasamy, 1987) agree on the inadequacy of the k–ε model to predict airflow patterns and underline its limitation by comparison with experimental data. According to Wilcox (1994) and Menter (1997) the k–ε model predicts significantly too high shear-stress levels and thereby delays or completely prevents separation. According to Launder et al. (1992) this trend can be more pronounced in the presence of adverse pressure gradient and leads to overprediction of the wall shear stress. Aude et al. (1998) pointed out the difficulty in accurately predicting the airflow characteristics concerning the velocity levels, the turbulent kinetic energy, its dissipation rate and the turbulent viscosity in the stagnant regions with the k–ε model.

Moureh and Flick (2005) and Hoang et al. (2000) consider that the Coanda effect governing the attachment of the jet on the ceiling was not well predicted by the k–ε model. According to Moureh, the standard k–ε model overestimates the Coanda effect of the wall jet and fails to predict its separation. Nady et al. (1995) also underlined the inability of the k–ε model to predict the detachment of the jet from the ceiling as observed experimentally under non-isothermal conditions. To improve numerical predictions in a ventilated enclosure with a strong Coanda-effect influence, Choi et al. (1990) suggested modifying the multiplier coefficient $C_\mu = 0.09$ of the turbulent viscosity given by the standard k–ε model.

In a comparison concerning indoor airflow, Chen (1995) tested five two-equation models: the standard k–ε model, a LRN k–ε model, a two-layer k–ε model, a two-scale k–ε model, and a renormalization group (RNG) k–ε model. The author concluded that any one of these two-equation models is able to predict the presence of the secondary recirculating flow. More recently, Moureh et al. (2002) and Moureh and Flick (2005) also tested and compared various turbulence closure models including the standard and the low Reynolds number form of the two-equation k–ε model, and the more advanced RSM. The author concluded that only RSM was able to accurately predict the separation of the jet from the wall and the general behaviour of airflow patterns related to the primary and to the secondary recirculations. This concerned loaded and unloaded long enclosures where the wall jet was subjected to an adverse pressure gradient and the turbulence anisotropy effect was pronounced.

In a comparative review, Nallasamy (1987) concludes that the use of RSM models to account for curvature effects, countergradient transport and secondary flows would improve the confidence in turbulence closure models. Karimipanah (1999) also recommends the use of second-moment closure turbulence models in order to better predict deflected corner flows where the effect of anisotropy of turbulence and streamline curvature are pronounced.

The purpose of this paper is to experimentally and numerically characterize the airflow patterns in a long enclosure ($L/H = 5.2$) ventilated by a ceiling wall-jet and loaded with two rows of empty slotted boxes (ESB). For the studied enclosure, inlet and outlet sections are located on the same side. Concerning the numerical approach, we felt it appropriate to explore the performance of the second-moment closures as well as the standard k–ε linear eddy viscosity model.

The investigation will concern the air velocity characteristics within the enclosure and the overall behaviour of airflow patterns throughout the load, above and around the ESB.

3. Experimental device

The main device used for this study was a reduced scale model of a trailer with a length scale ratio of 1/3.325. Airflow inlet and outlet were located in the front face of the parallelepiped as shown in Fig. 1 where is represented the full-scale geometry. All dimensions and results in this paper are given in connection with the full-scale geometry using the Reynolds analogy. The walls of the scale model were composed of wood except one side constructed of glass to allow laser-Doppler velocimetry. The mean velocity and its fluctuations were obtained with a one-dimensional anemometer, which comprised a 50 mW laser diode emitting a visible red beam at 690 nm wavelength, a beam splitter, a Bragg (acousto-optic) cell, a focusing and receiving lens to collect scattered light from the measurement point and a photomultiplier. The flow to be measured must contain particles from an atomizer that scatters light as the flow carries them through the measurement volume. The probe was carried on an automatic displacement system.

The slot-ventilated enclosure was supplied with air from a centrifugal turbine, which can go up to 5800 m^3/h. The airflow was introduced in the enclosure perpendicular to the front face with a mean velocity of $U_0 = 11.5$ m/s, that is a Reynolds number of 1.9×10^5 and a relative standard

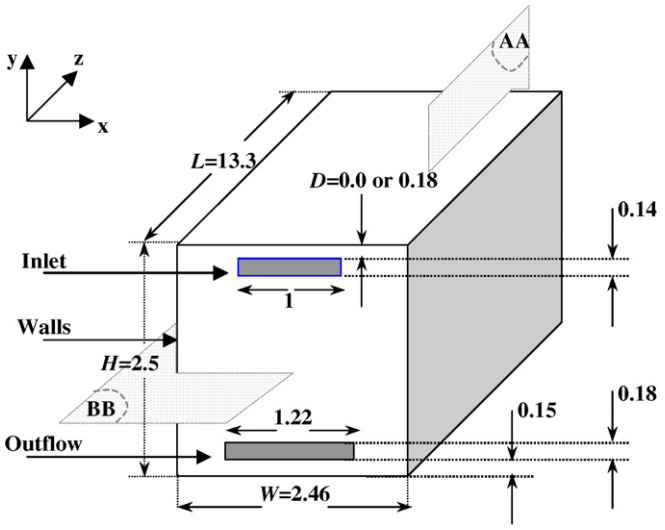

Fig. 1. Dimensions of the enclosure (m).

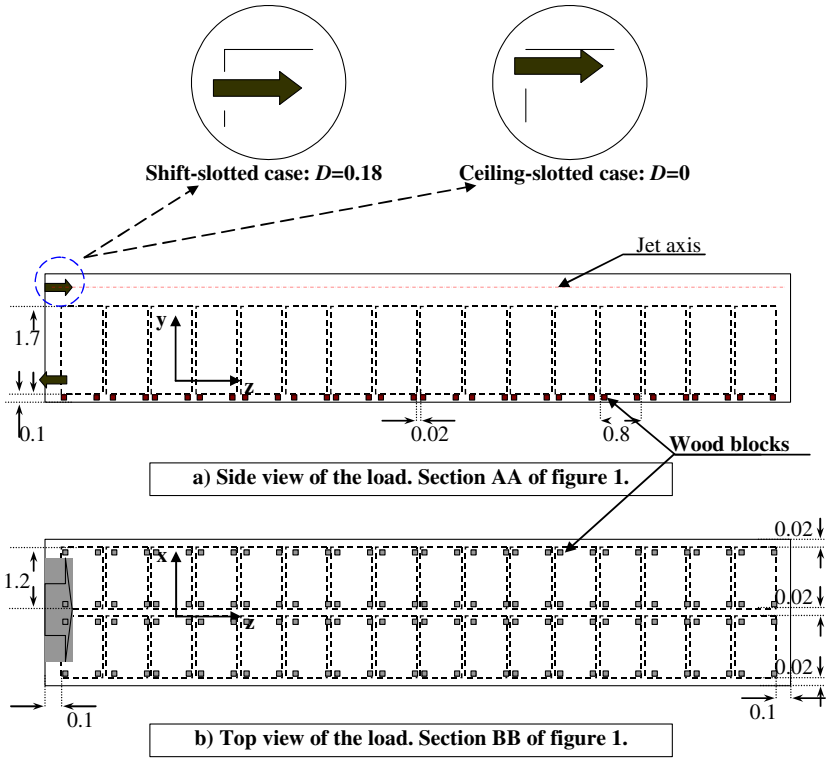

Fig. 2. Configuration of the load in the enclosure.

deviation I_{0z} of 10%. The two inlet configurations studied were the ceiling slotted case ($D = 0$, D is the distance of the jet inlet slot below the ceiling) and the downwards displace slot case ($D = 0.18$ m) with the same load. These configurations were performed in the current study to allow comparisons with previous data.

The enclosure was loaded with 2 rows of 32 polystyrene slotted boxes of size $1.8 \times 0.8 \times 1.2$ m (Fig. 2). The slots were spread over the six faces of each box and give to air 15% of the surface to go through. The boxes were set down on wood blocks of dimension $0.1 \times 0.1 \times 0.1$ m allowing air circulation under the load. Small gaps of 0.02 m were maintained between the boxes.

4. Modelling approach

4.1. Governing equations

The time-averaged Navier–Stokes differential equations for steady, high-Reynolds numbers and incompressible flows expressed in their conservative form for mass and momentum conservation were solved by a finite volume method using the Fluent solver.

Turbulence was predicted with the standard k–ε turbulence model as described by Launder and Spalding (1972) and the Reynolds Stress Model (RSM) as described by Launder (1989), which is an advanced model for which an individual transport equation is derived for each shear stress component. The RSM was used as the default turbulence model.

To obtain the transport equations for Reynolds turbulent stress we multiply the i-component Navier–Stokes equation for the instantaneous velocity $(U_i + u_i)$ by the fluctuation u_j. We then add u_i times the equations for $(U_j + u_j)$, and average. This gives rise to:

$$U_k \frac{\partial \overline{u_i u_j}}{\partial x_k} = -\frac{\partial}{\partial x_k}\left[\overline{u_i u_j u_k} + \frac{p}{\rho}(\delta_{kj}u_i + \delta_{ik}u_j) - \nu\frac{\partial(\overline{u_i u_j})}{\partial x_k}\right] + G_{ij} + \frac{p}{\rho}\overline{\left[\frac{\partial u_i}{\partial x_j} + \frac{\partial u_j}{\partial x_i}\right]} - 2\nu\overline{\frac{\partial u_i}{\partial x_k}\frac{\partial u_j}{\partial x_k}} \quad (2)$$

where $G_{ij} = -\overline{u_i u_k}\frac{\partial U_j}{\partial x_k} - \overline{u_j u_k}\frac{\partial U_i}{\partial x_k}$ represents the production term

The diffusive transport term was represented by a simplified form of the generalized gradient diffusion hypothesis as:

$$-\frac{\partial}{\partial x_k}\left[\overline{u_i u_j u_k} + \frac{p}{\rho}(\delta_{kj}u_i + \delta_{ik}u_j) - \nu\frac{\partial(\overline{u_i u_j})}{\partial x_k}\right] = \frac{\partial}{\partial x_k}\left(\frac{\nu_t}{\sigma_k}\frac{\partial}{\partial x_k}(\overline{u_i u_j})\right) \quad (3)$$

The pressure–strain term consisted of the linear return-to-isotropy and is modelled by Launder et al. (1975) as:

$$\overline{\frac{p}{\rho}\left[\frac{\partial u_i}{\partial xj} + \frac{\partial u_j}{\partial xi}\right]} = -C_1\frac{\varepsilon}{k}\left[\overline{u_i u_j} - \frac{2}{3}\delta_{ij}k\right] - C_2\left[G_{ij} - \frac{2}{3}\delta_{ij}G\right] + \phi_{ij,w} \quad (4)$$

where:

- $\phi_{ij,w}$ represents the wall reflection term as described by Gibson and Launder (1978) and based on the normal distance to the wall;
- the constants $C_1 = 1.8$ and $C_2 = 0.60$, and $G = 0.5\ G_{ii}$.

The dissipation term was assumed isotropic, and was approximated by:

$$2\nu\overline{\frac{\partial u_i}{\partial x_k}\frac{\partial u_j}{\partial x_k}} = \frac{2}{3}\partial_{ij}\varepsilon \tag{5}$$

where the dissipation rate was computed via the ε transport equation (Launder and Spalding, 1972).

4.2. Boundary conditions

The flow rate was set at 11.5 m/s at the inlet corresponding to about 70 air-renewals by hour in the enclosure. The inlet turbulence parameters were obtained from the measurements assuming isotropy. The boundary conditions are summarized in Table 1.

In Table 1, indices (τ, η, λ) represent the local coordinate system of the wall, where τ is the tangential coordinate, η is the normal coordinate, and λ is the binormal coordinate. Then the local Reynolds stresses at the wall-adjacent cells were computed using the wall kinetic energy.

The values of k used at the boundaries are obtained from a transport equation of turbulence kinetic energy similar to the one in the standard k–ε model. For reasons of computational convenience, this equation is solved globally (on the domain), even though the values of k thus computed are needed only near the wall. The boundary condition for k imposed at the wall is

$$\frac{\partial k}{\partial n} = 0 \tag{6}$$

where n is the local coordinate normal to the wall.

The production of kinetic energy, and its dissipation rate, ε, at the wall-adjacent cells, which are the source terms in the k equation, are computed on the basis of the local equilibrium hypothesis.

The specifications of the near-wall cells are 6×10^{-3} m, 1.4×10^{-2} m and 7×10^{-3} m respectively in the directions x, y and z. The growth ratio between two adjacent cells does not exceed 20%. Due to the high variations velocities on the whole ceiling, the y^+ varies between 3 and 300. Consequently, some cells are located within the viscous sublayer whereas other cells are located in the logarithmic zone. To overcome this difficulty, a hybrid wall treatment guaranteed the correct asymptotic behaviour for large and small values of y^+ and reasonable representation of velocity profiles in the cases where y^+ falls inside the buffer region. It's a near-wall modelling method that combines a two-layer model with enhanced wall functions. This was obtained by blending linear (viscous-sublayer) and logarithmic (turbulent) laws-of-the-wall using a function suggested by Kader (1993).

The mean velocity at the walls is calculated as follow:

$$u^+ = \mathrm{e}^{\Gamma}u^+_{\mathrm{vis}} + \mathrm{e}^{1/\Gamma}u^+_t \tag{7}$$

where Γ is define by Kader (1993) as a function of y^+ and wall roughness. and:

$$u^+_{\mathrm{vis}} = y^+, \quad u^+_t = \frac{1}{\kappa}\ln(Ey^+) \tag{8}$$

In this equation $E = 9.793$.

It's a near-wall formulation that can be used with coarse meshes as well as fine meshes.

4.3. Modelling the slotted wall

Fluid flow was sensitive to the slotted wall effect by the means of the normal pressure jump through the wall, which is characterized by C_1 the pressure loss coefficient:

$$\Delta P = \frac{1}{2}C_1\rho U^2_{\perp} \tag{9}$$

where ΔP is the total pressure drop and $U_\perp$ is the mean velocity normal to the wall. The pressure drop for a single slotted wall was measured and the coefficient C_1 equals 80. But some couples of walls were separated by small gaps. Considering that two slotted walls pressed against each other give about the same pressure drop to the flow as a single one (if the slots are perfectly aligned), we considered that the pressure drop coefficient for one slotted wall that is very close to another (C_2) is reduced to the half compared to a single one:

$$C_2 = \frac{C_1}{2} \tag{10}$$

Table 1
Summary of the boundary conditions

	Velocity	Pressure	Turbulence
Inlet	$U_x = U_y = 0$ m/s $U_z = 11.5$ m/s	–	$k_0 = 3/2(U_0 I_{0z})^2; I_{0z} = 10\%$ $\varepsilon_0 = C_\mu^{0.75}k_0^{1.5}/0.07D_{\mathrm{H}};\ D_{\mathrm{H}} = 0.2$
Outflow	–	Constant pressure	–
Walls	$U_x = U_y = U_z = 0$ m/s	–	$\frac{u_\tau^2}{k} = 1.098; \frac{u_\eta^2}{k} = 1.098$ $\frac{u_\lambda^2}{k} = 0.655; \frac{u_\eta u_\tau}{k} = -0.255$
Symmetry	Zero normal gradient for all variables		

To support this hypothesis, Fig. 3 shows the evolution of pressure drop coefficient for two parallel slotted walls depending on the separation distance between them. The measurements showed that when the separation distance tends to zero, the two walls are equivalent to a single wall. The pressure drop coefficients are set at the boundaries faces of the boxes domain as shows in Fig. 4.

4.4. Modelling the boxes interstices

As there was a big difference between boxes dimensions and the small gaps between them (Fig. 2b), direct meshing of all these gaps would lead to very large grid size (exceeding the memory capacity) and a high computing time, especially if we want to apply a gradual grid refinement where the size ratio between two consecutive cells should not exceed 20%.

To avoid this difficulty, we replaced thin air spaces between boxes along the vehicle by a fictitious, aerodynamically equivalent, porous medium for which the permeability coefficient was chosen so as to ensure the same airflow resistance as the actual medium. This approach was made possible because air velocity measurements showed that laminar flow was dominant between boxes ($Re < 500$) (Menia, 2001). Consequently, there is a linear relationship between airflow rate and pressure gradient as in a porous medium governed by Darcy's law.

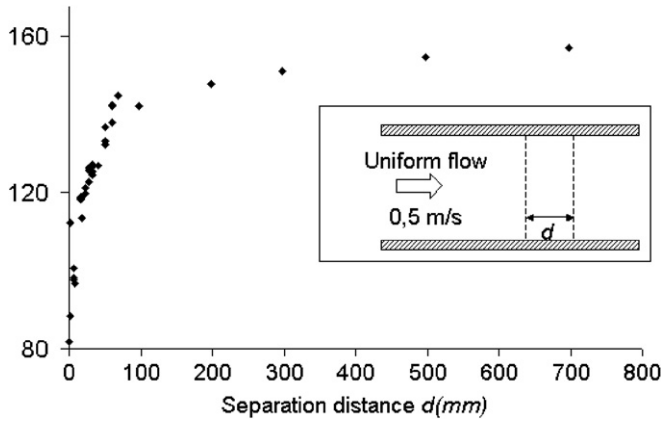

Fig. 3. Pressure drop coefficient throughout two slotted walls as a function of walls' separation distance (d).

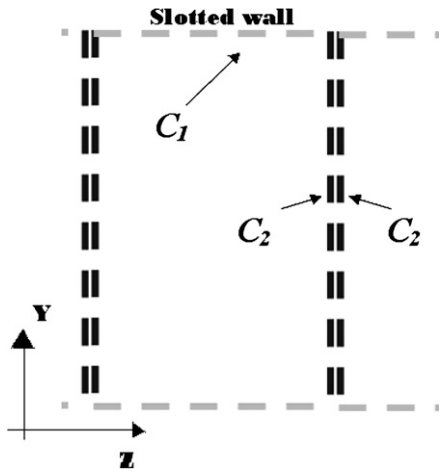

Fig. 4. Setting the pressures drop coefficients for the slotted walls of one pallet.

In the proposed method, the permeability coefficient for this fictitious porous medium was chosen in order to ensure that for a given pressure gradient, the same flow rate as for the actual medium is obtained. Consequently, the analogy between the laminar flow between two parallel plates separated by a distance e and a flow in a porous medium between two parallel plates separated by a distance e' are related as follows:

$$(U_{\text{mean}} \times e)_{\text{actual medium}} = (U_{\text{mean}} \times e')_{\text{porous medium}} \Rightarrow \left(\frac{\mathrm{d}p}{\mathrm{d}x}\frac{e^2}{12\mu}\right)e = \left(\frac{K_{\text{p}}}{\mu}\frac{\mathrm{d}p}{\mathrm{d}x}\right)e' \qquad (11)$$

Thus the equivalent permeability is equal to:

$$K_{\text{p}} = \frac{e^3}{12e'} \qquad (12)$$

The use of this analogy allows the reduction in grid size because air spaces separating boxes were represented by relatively large porous cells ($e' = 0.06$ m) with a permeability coefficient that was calculated from Eq. (12). Fig. 5 illustrates the effect of this analogy on grid refinement and consequently on grid size.

Up to 830,000 cells were used to perform the simulations. The solutions proved to be practically insensitive to grid size from 300,000 cells.

5. Results and discussion

The results are organized into three main parts:

- the first part presents the jet diffusion in the enclosure loaded with slotted boxes;
- the second part discusses the load influence making comparisons with the empty case of Moureh et al. (2002) and the impermeable load of Menia (2001). This comparison highlights the load porosity effect on the jet diffusion;
- the last part compares experimental and numerical results in function of turbulence handling in CFD for enclosed jet simulation.

5.1. Jet flow description using the slotted boxes

Figs. 6 and 7 plot, for the downshifted case ($D =$ 0.18 m), the contour levels of longitudinal normalized velocity U_z/U_0 in the symmetry plane and in the inlet-centred horizontal plane respectively. They lead to several conclusions on the general pattern of the jet.

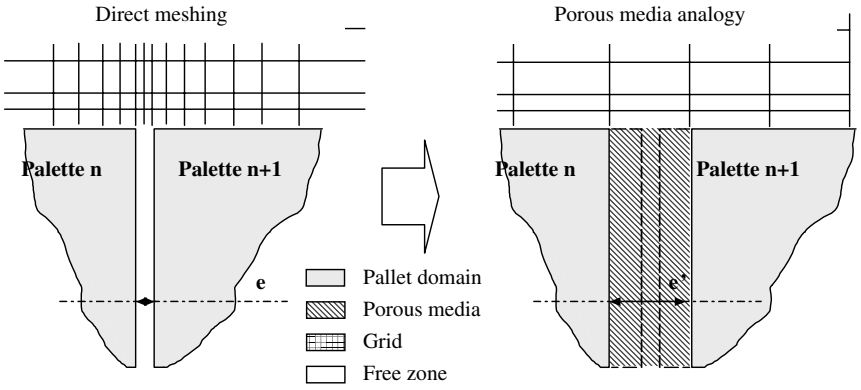

Fig. 5. Analogy between laminar flow and porous medium flow on the grid refinement.

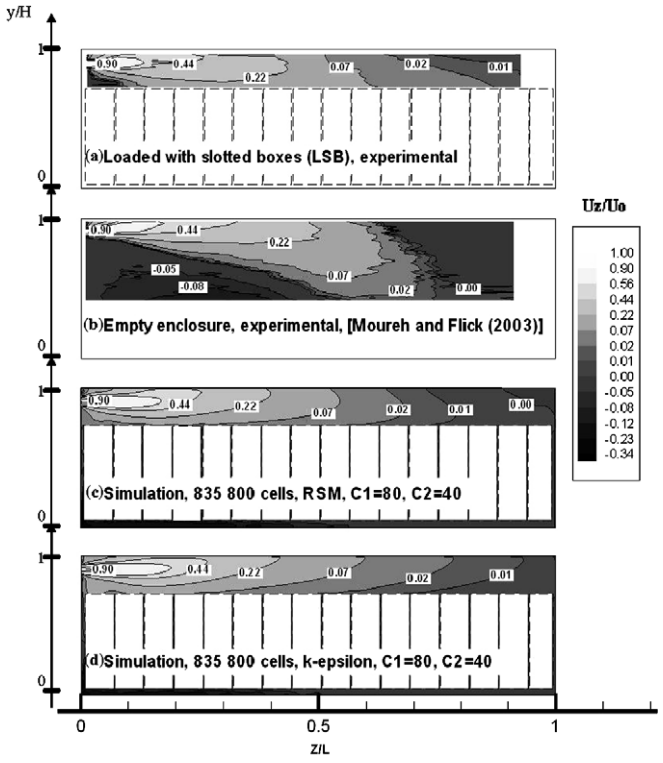

Fig. 6. Contours levels of longitudinal normalized velocity U_z/U_0 in the symmetry plane (downshifted case: $D = 0.18$ m).

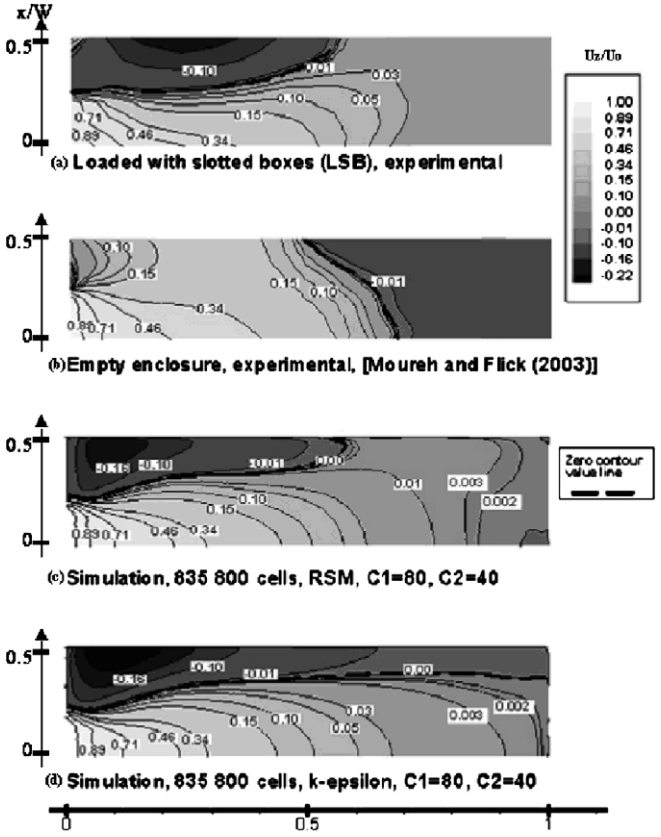

Fig. 7. Contours levels of longitudinal normalized velocity U_z/U_0 in the inlet-centered horizontal plane (downshifted case: $D = 0.18$ m).

The results show a high degree of heterogeneity in term of airflow and velocity levels within the enclosure. The high velocities and steep gradients observed in the front part $z/L \in [0, 0.5]$, contrasted with the stagnant zone, in the rear part $z/L \in [0.5, 1]$.

Due to the confinement effect, two lateral vortices structures were induced by the jet intrusion into the enclosure as it can be seen in Fig. 7a (negative values of U_z). These structures controlled the initial growth of the jet and limited its diffusion in the transverse direction.

In the streamwise/longitudinal direction, the jet attaches rapidly the ceiling by the Coanda effect. Further downstream, the free layer of the wall jet attaches the top of the pallets and flows onto it to the rear.

5.2. Jet characteristics

Figs. 8–12 show the evolution of the jet characteristics in the symmetry plane related to the normalized velocity U_z/U_0, static pressure, turbulence of z-velocity, jet trajectory and the maximum velocity ($U_{z\max}$) respectively.

In the inlet region $z/L \in [0, 0.15]$, the strong decay of velocity on the jet axis (normalized velocity decreases from 1 to 0.6) could be partially explained by the jet deflection to the ceiling. Due to this mechanism, the geometrical jet axis is first in the potential core but further downstream it is sit-

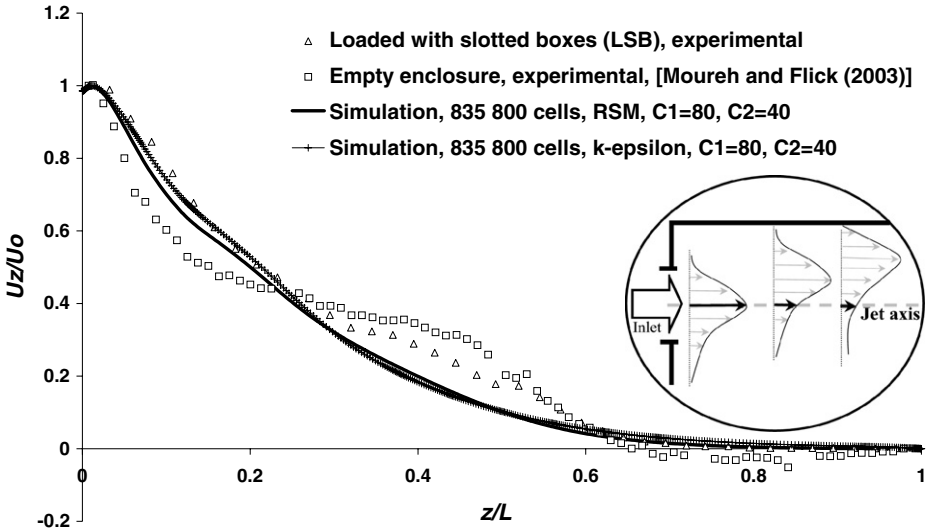

Fig. 8. Evolution of the longitudinal velocity on the jet axis along the enclosure (downshifted case: $D = 0.18$ m).

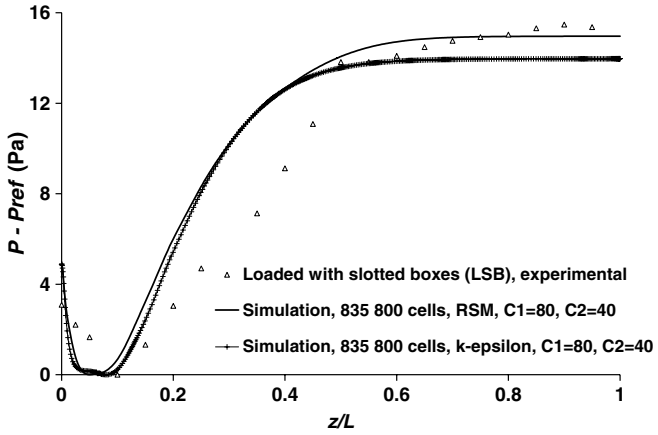

Fig. 9. Static pressure on the jet axis in the enclosure loaded with slotted boxes (downshifted case: $D = 0.18$ m).

uated in the outer layer where lower velocities are present (Fig. 8). This deflection also explained the peak in z-velocity turbulence observed on Fig. 10 as it tends to approach the jet mixing layer, where turbulence is generated, from the jet axis. In this zone, the decay of the maximal velocity followed the characteristic decay of the theoretical 2D unbounded wall jet until $z/L = 0.2$ (Fig. 12b). This trend confirmed the results of Yu et al. (2003) obtained in shorter enclosures.

In the intermediate region $z/L \in [0.15, 0.5]$, due to the confinement effect, the static pressure increased by 14 Pa in this area (Fig. 9). The decay of maximal velocity in the symmetry plane is stronger than one predicted for the theoretical 2D wall jet as presented in Fig. 12. This reflects, the cumulative effect due to the adverse pressure gradient (Fig. 9) and to the lateral interactions with the return flow (Fig. 7a). The both mechanisms strongly affect the jet development and caused it to vanish at $z/L = 0.5$ approximately.

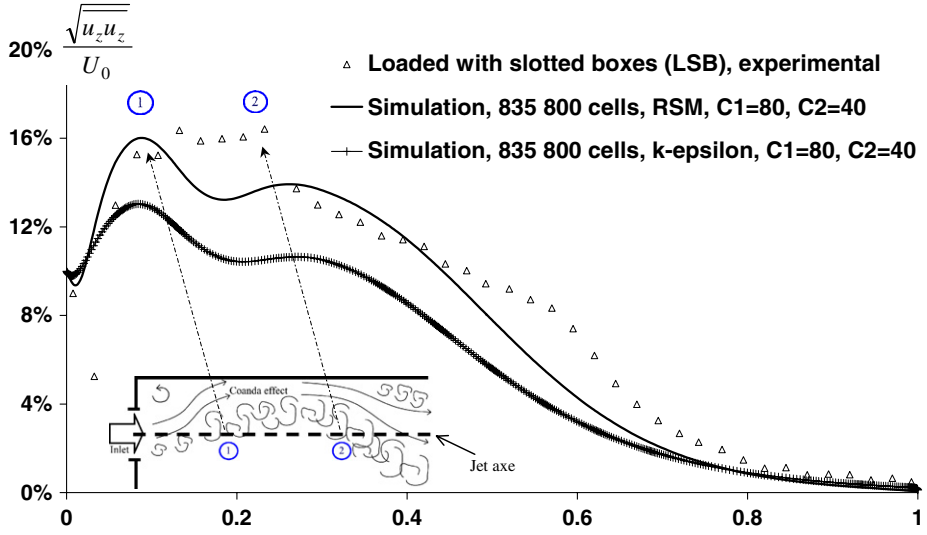

Fig. 10. Normalized turbulence of z-velocity $\sqrt{\overline{u_z u_z}}/U_0$ on the jet axis (downshifted case: $D = 0.18$ m).

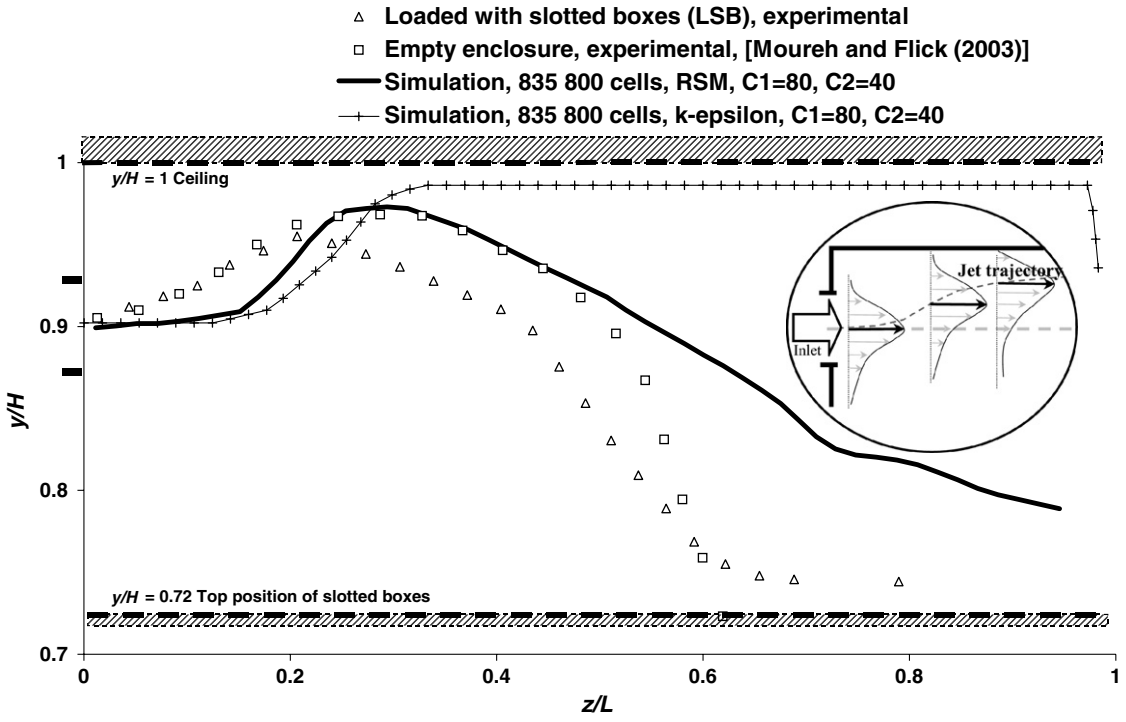

Fig. 11. Jet trajectory in the symmetry plane (y_{max} vs. z) (downshifted case: $D = 0.18$ m).

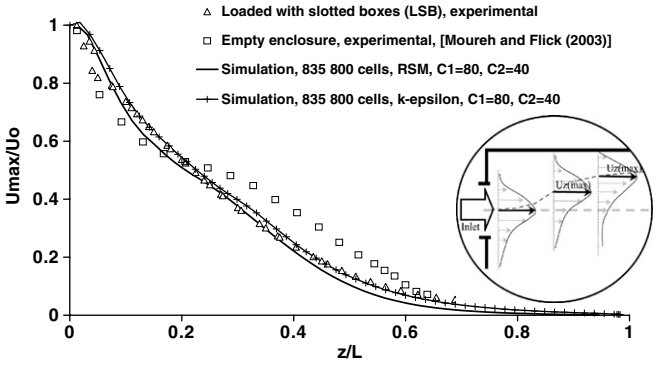

(a) Comparison with the empty case and numerical simulations

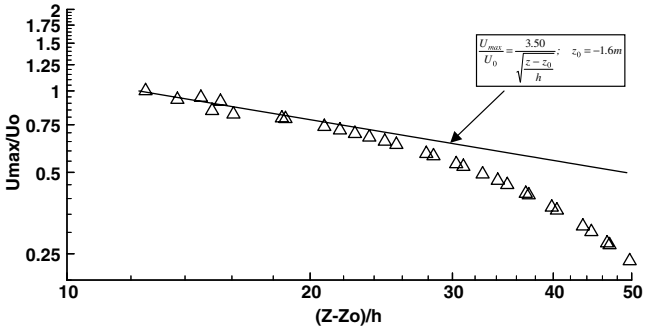

(b) Comparison of LSB with the theorical 2D wall jet [Rajaratnam. 1976]

Fig. 12. Maximum velocity evolution in the symmetry plane (U_{zmax} vs. z) (downshifted case: $D = 0.18$ m).

In the rear region ($z/L \in [0.5, 1]$), flow is weak; U_z velocity levels were less than $0.2 \times U_0$ (Figs. 6 and 7), from $z/L > 0.7$ these levels did not even exceed 5% of U_0. Velocity fluctuation also decreased in this zone (Fig. 10). The uniform static pressure level observed in this area (Fig. 9) also reflects the presence of stagnant zone.

5.3. Comparison with other configurations

This section describes the load influence making comparisons with the empty case of Moureh et al. (2002) and the case of impermeable load (Menia (2001)). The ceiling-inlet distance D was different for these two configurations. But the experiments with the slotted boxes in the current study were performed for the two distances to allow comparisons with the previous data.

The data used in these discussions are summarized in Table 2.

It is important to note that with the slotted boxes, airflow patterns were nearly the same for $D = 0$ and $D = 0.18$ m, with the exception of the Coanda effect at the ceiling level.

5.4. Comparing with the empty enclosure flow

Figs. 6–12 give a comparison between the empty enclosure case of Moureh et al. (2002) and the present loaded case (LSB).

Moureh et al. (2002) showed clearly that the wall jet separates from the ceiling at approximately 70% of the empty enclosure length. This separation splits the jet into two regions dominated by two vortices of opposite circulation (cf. negative values of U_z at the rear, Fig. 8). But in our case, the velocity tended asymptotically to zero but remained positive on the jet axis even if there was an adverse pressure gradient from $z/L = 0.1$ to the rear. This means that no recirculating pattern occurred in the symmetry plane.

Fig. 7 plots the contour of U_z/U_0 on the inlet centered horizontal plane and shows a major difference in jet diffusion between the empty (Fig. 7b) and the loaded case (Fig. 7a). In the empty enclosure there was a head-on flow moving forward and occupying the full width of the enclosure from $z/L = 0.1$ to $z/L = 0.5$. But in the slotted boxes case, the geometrical confinement effect due to the presence of the load was reinforced dynamically by the two lateral vortices, which tended to reduce the jet diffusion and leaded to a centered flow. As a consequence, the inlet decay of the jet ($z/L \in [0, 0.15]$), in the empty case is higher than in the loaded case. For $z/L \in [0.15, 0.5]$ the tendency was inversed, the decay in the loaded case was higher than in the empty case. The load limited the entrainment flow and hence, tended to decrease the velocity level on the jet axis.

Table 2
Summary of experimental results

	Empty configuration	Loaded with slotted boxes	Loaded with impermeable boxes
Downshifted case ($D = 0.18$ m)	Moureh et al. (2002)	Current study	-
Ceiling slotted case ($D = 0$)	-	Current study	Menia (2001)

Although these differences in recirculating patterns, Figs. 6–8 show quite the same velocity levels along the enclosure for the empty and loaded cases. Both cases presented a stagnant zone in which the flow was weak at the rear. Low velocities and low exchange with the rest of the enclosure characterized this zone.

5.5. Comparing with the case of impermeable boxes

To highlight the load porosity effect on the airflow pattern and the jet behaviour, experimental longitudinal velocity concerning slotted boxes (SB) and impermeable boxes (IB) (Menia (2001)), were compared in Fig. 13. These comparisons concerns three cross sections of the enclosure above the boxes: $z/L = 1/4$, $z/L = 1/2$ and $z/L = 3/4$. Contours of U_z/U_{max} are presented and U_{max} is the maximum of $|U_z|$ in each section.

In the three sections, higher positive velocities were observed in the SB case. In the first quarter for example, the values of U_{max}/U_0 are 50% and 30% for SB and IB respectively. This clearly indicates that the boxes porosity contributes to a better wall jet development along the enclosure by enabling the airflow entrainment through the load. In addition, the impermeability of the load (IB case) tend to confine the return flow principally above the boxes as shown in Fig. 13 where higher negative velocity values are observed in the IB case. For this configuration there are higher velocity gradients between the two opposed streams and consequently more aerodynamic interaction and friction between them. This aspect also limits the wall jet development in the IB case.

As a consequence, the jet separates from the ceiling and attaches to the top of the pallets in the IB case at $z/L = 1/2$. On the contrary in the SB case, the jet occupies progressively the full width above the pallets can be seen at $z/L = 3/4$. Obviously, the return flow took place partially within the load in the SB case.

Other local aspects concerning airflow patterns could be noticed in Fig. 13:

- At z/L=1/4, the two cases presented a reverse flow on the wall sides.
- At $z/L = 1/2$ in the IB case due to the wall jet separation, the velocity varied principally from the top of the boxes, where the wall jet attached by Coanda effect flowed to the rear, to the ceiling ($U_z > 0$), where reverse flow took place ($U_z < 0$). This reveals a vertical recirculation bubble, which occupies the full width of the enclosure. With the slotted boxes, the velocity varied principally from the centre, where $U_z > 0$, to the lateral side, where $U_z < 0$. This reveals a horizontal recirculation bubble, which occupies the full height above the boxes.
- At $z/L = 3/4$: With the impermeable boxes (Fig. 13b), air was almost stagnant; the maximum U_z velocity was very low ($U_{max}/U_0 = 0.5\%$). With the permeable boxes (Fig. 13a) the velocity levels remained significant

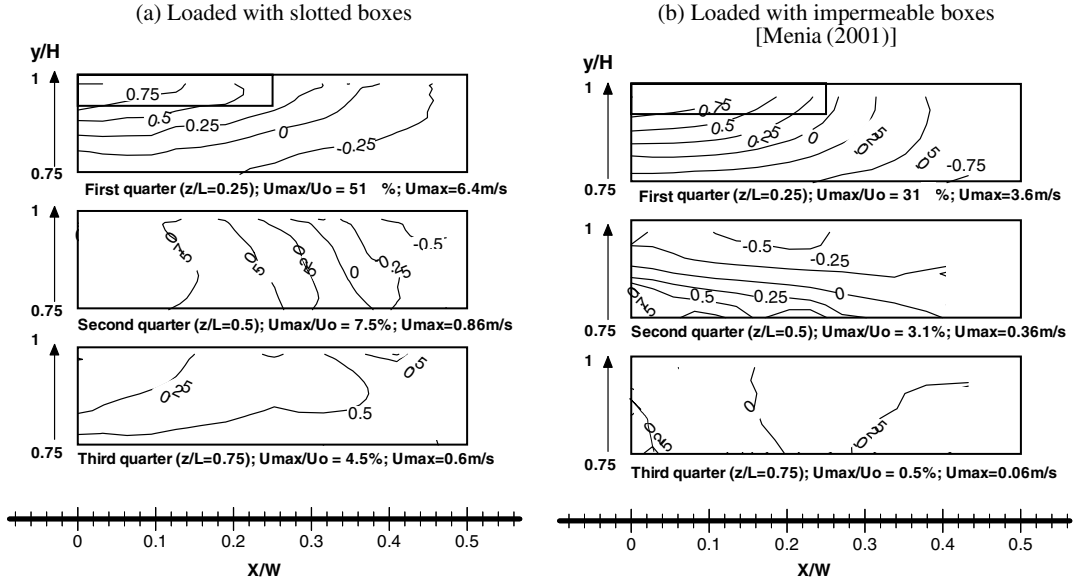

Fig. 13. Contour plots of U_z/U_{max} in transversal sections along the enclosure (ceiling-slotted case: $D = 0.18$ m).

($U_{max}/U_0 = 4.5\%$) without reverse flow ($U_z > 0$). This confirmed a better wall jet development and penetration into the enclosure for SB case.

These conclusions clearly embody the importance of load porosity on the jet behaviour. Fig. 14 shows the approximative outlines of air patterns for the different configurations.

5.6. Comparing with the numerical results

The simulations were implemented using the FLUENT solver. Two turbulent models were compared and contrasted: the standard k–ε turbulence model and the Reynolds Stress Model (RSM).

In high velocity zones, no great differences were found between k–ε and RSM in terms of velocity prediction. Figs. 6–12 and 15 show that when $z/L < 0.5$ the two models gave practically the same results. The relative error compared with experimental results did not exceed 10% of U_0 for both turbulence models. However, this difference increased in lower velocity areas located in the rear and further away from the symmetry plane. This could be explained by the low level of velocities and to their instabilities in the stagnant zones where no main flow is identified.

However, it should be noticed that the major difference between the two models concerns the jet behaviour rather than local velocity values.

Concerning the jet attachment on the ceiling by Coanda effect in the inlet area, the k–ε model underestimated the jet deflection. The adherence point, defined as the location of the highest point of jet trajectory, was located, at $z/L = 0.35$ instead of 0.25 for the experiment (Fig. 11). This

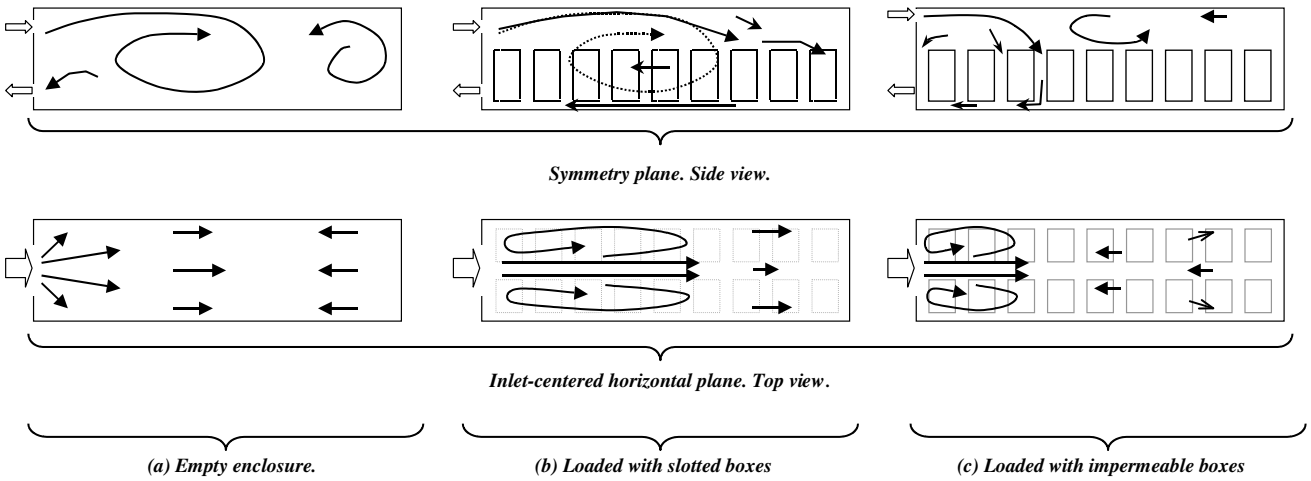

Fig. 14. Approximative outlines of air patterns, comparison between the empty enclosure and the loaded cases.

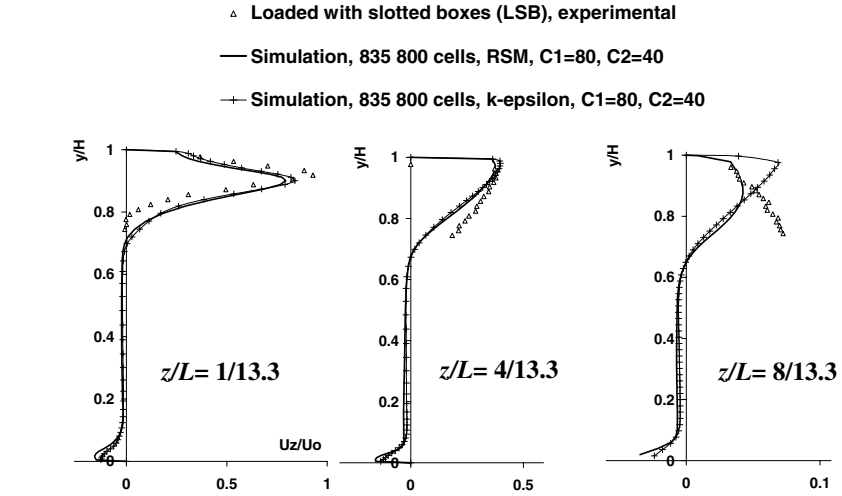

(a) Uz/Uo profiles in the symmetry plane for lines z=1m. z=4m and z=8m

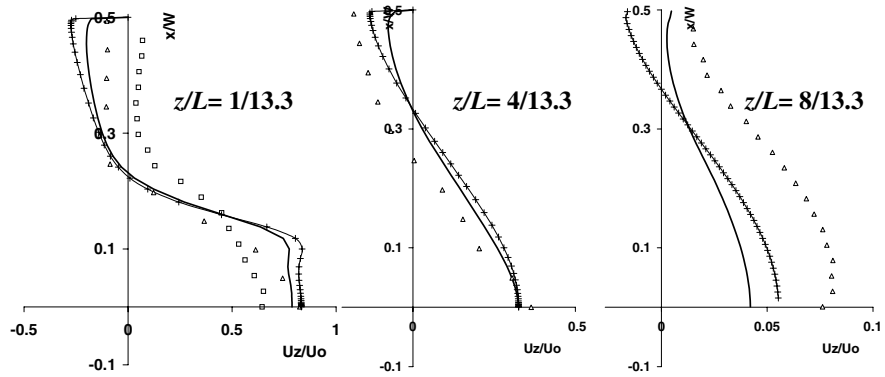

(b) Uz/Uo profiles in the horizontal jet plane for lines z=1m. z=4m and z=8m

Fig. 15. U_z/U_0 profiles on vertical and horizontal lines.

way the jet potential core predicted by simulation was less deflected and this explains the higher velocity on the jet axis compared to with experiments (Fig. 8). Use of RSM results in a stronger jet deflection and the adherence point was relatively better predicted at $z/L = 0.3$ (Fig. 11).

Further downstream, the jet trajectory predicted by the k–ε model was still close to the ceiling while experimental data showed a detachment from this wall followed by a deflection towards the top faces of the pallets by Coanda effect (Fig. 15a). This clearly indicates that the k–ε model lacks sensitivity with respect to the adverse pressure gradient, over-predicts the ceiling Coanda effect (Fig. 6d) and hence increases the jet penetration distance into the enclosure. This could explain the higher velocities obtained by this model, notably in the rear. On the contrary, the RSM better performed the partial jet detachment from the ceiling and its progressive deflection towards the top of the pallets. However, the aerodynamic interaction between the jet and the slotted wall need to be improved by taking into account the horizontal frictional resistance exerted by the top of the pallets against the jet. Although, this horizontal friction could be neglected in terms of pressure losses compared with the perpendicular effect, it becomes essential for the numerical model to be able to predict the jet attachment on the top of the pallets by Coanda effect as it can be seen experimentally in Figs. 6 and 11.

Experimental and RSM predictions showed that the area of the lateral vortex structures, delimited by the 0 velocity contour, are confined near the inlet section in the front part of the enclosure (Fig. 7). The k–ε model predicts more stretched structures covering the whole side wall from the front to the rear. This could be explained by the high rate of entrainment flow predicted by this model (data not shown) due to its greater, but not physically, jet stability and penetration along the enclosure.

However, it should be stated that neither model agrees closely with the shape of the contours. While experiments showed that lateral vortices affect and slightly predominate jet diffusion, both models display an inversed tendency.

Another aspect displayed by experimental data concerns the evolution of the horizontal velocity contours along the enclosure. These contours show that the maximum of the jet velocity still in the symmetry plane up to $z/L = 0.5$. Further downstream, the jet tends to deviate towards the lat-

eral walls and brings out a curved velocity profile on the axis as shows Fig. 7. RSM reflects qualitatively this tendency, whereas the k–εfails to predict this deviation.

6. Conclusion

Experiment on a reduced scale model and CFD simulation were performed to study an enclosure loaded with slotted boxes supplied by a ceiling-jet. The aim was to characterize the airflow patterns in a typical refrigerated truck configuration. Making comparisons of this configuration with empty enclosures and impermeable boxes load made it possible to highlight the load effect on the jet diffusion. The main conclusions were:

- the load modified strongly the flow patterns but the velocity levels remained similar in all cases: jet velocity decreased rapidly in the first half and in the rear half the velocity was low ($|U_z| < 10\%U_0$);
- the jet penetration and the main recirculating flow were reduced as the load porosity decreased;
- the sideways diffusion was reduced as the porosity of the load decreased. The loaded cases presented a back flow on the sides of a centred jet;
- there was no recirculation at the rear part in the case of the slotted box load.

Numerical prediction using the RSM turbulence model gave satisfactory results; it took into account for example, the ceiling Coanda effect, lateral recirculation, jet decay and pressure behaviour. However, the Coanda effect at the top of the boxes could be better predicted if the model includes the wall friction on the slotted walls.

Acknowledgements

The authors thank the Ile de France region and the French Ministry of Agriculture, Food, Fisheries and Rural Affairs for their support and funding of this work through an AQS project.

References

Adre, N., Albright, L.D., 1994. Criterion for establishing similar air flow patterns (isothermal) in slotted-inlet ventilated enclosures. Transactions of the ASAE 37, 235–250.

Aude, P., Béghein, C., Depecker, P., Inard, C., 1998. Perturbation of the input data of models used for the prediction of turbulent air flow in an enclosure. Numerical Heat Transfer, Part B 34, 139–164.

Awbi, H.B., 1989. Application of computational fluid dynamics in room ventilation. Building and Environment 24 (1), 73–84.

Bjerg, B., Svidt, K., Zhang, G., Morsing, S., Johnsen, J.O., 2002. Modeling of air inlets in CFD prediction of airflow in ventilated animal houses. Computers and Electronics in Agriculture 34 (1-3), 223–235.

Bushmann, P., Ribérion, J., Millet, J.R., 1994. Numerical prediction of airflow patterns in large enclosures with supplied air jet system. In: Proceedings ROOMVENT'94, Air Distribution in Rooms, Fourth International Conference, vol. 1, 15–17/06/94, Krakow POL.

Chen, Q., 1995. Comparison of different k–ε models for indoor air-flow computations. Numerical Heat Transfer Part B-Fundamentals 28 (3), 353–369.

Choi, H.L., Albright, L.D., Timmons, M.B., Warhaft, Z., 1988. An application of the k–ε turbulence model to predict air distribution in slot ventilated enclosure. Transactions of the ASAE 31 (6), 1804–1814.

Choi, H.L., Albright, L.D., Timmons, M.B., 1990. An application of the k–ε turbulence method to predict how a rectangular obstacle in a slot-ventilated enclosure affects air flow. Transactions of the ASAE 33 (1), 274–281.

Craft, T.J., Launder, B.E., 2001. On the spreading mechanism of the three-dimensional turbulent wall jet. Journal of Fluid Mechanics 435, 305–326.

Davidson, L., 1989. Ventilation by displacement in a three-dimensional room: a numerical study. Building and Environment 24, 263–272.

El Hadidi, B.M.N., 1998. A computational study of flow in mechanically ventilated space. Faculty of Engineering, Cairo University, Giza Egypt.

Gebremedhin, K.G., Wu, B.X., 2003. Characterization of flow field in a ventilated space and simulation of heat exchange between cows and their environment. Journal of Thermal Biology 28, 301–319.

Gibson, M.M., Launder, B.E., 1978. Ground effects on pressure fluctuations in the atmospheric boundary layer. Journal Fluid Mechanics 86, 491–511.

Hoang, M.L., Verboven, P., De Baerdemaeker, J., Nicolai, B.M., 2000. Analysis of the air flow in a cold store by means of computational fluid dynamics. International Journal of Refrigeration 23 (2), 127–140.

Hoff, S.J., Janni, K.A., Jacobson, L.D., 1992. Three-dimensional buoyant turbulent flows in a scaled model, slot-ventilated, livestock confinement facility. American Society of Agricultural Engineers 35, 671–686.

Kader, B., 1993. Temperature and concentration profiles in fully turbulent boundary layers. International Journal of Heat Mass Transfer 24 (9), 1541–1544.

Karimipanah, T., Sandberg, M., 1994. Deflection and influence of room-size of a two-dimensional wall jet in a ventilated room. In: Fourth International Conference of Air Distribution in Rooms, ROOMVENT'94, June 15–17, Krakow, Poland.

Karimipanah, M.T., 1999. Deflection of wall jets in ventilated enclosures described by pressure distribution. Building and Environment 34, 329–333.

Lamers, A., Van de Velde, R., 1989. Airflow patterns in ventilated rooms. Phoenics Journal 2, 219–238.

Launder, B.E., Spalding, D.B., 1972. Lectures in Mathematical Models of Turbulence. Academic Press, London, England.

Launder, B.E., Spalding, D., 1974. The numerical computation of turbulent flows. Computer Methods in Applied Mechanics and Engineering 3, 269–289.

Launder, B.E., Reece, G.J., Rodi, W., 1975. Progress in the development of a Reynolds stress turbulence closure. Journal of Fluid Mechanics 68, 537–566.

Launder, B.E., 1989. Second-moment closure: present... and future? International Journal of Heat Fluid Flow 10 (4), 282–300.

Launder, B.E., 1992. On the modeling of turbulent industrial flows. In: Hirsch et al. (Eds.), Proceedings of Computational Methods in Applied Sciences. Elsevier, pp. 91–102.

Lindqvist, R., 1998. Reefer hold air distribution. I.I.F.-I.I.R. Commissions D1, D2/3, Cambridge, UK.

Mariotti, M., Rech, G., Romagnoni, P., 1995. Numerical study of air distribution in a refrigerated room. In: 19th International Congress of Refrigeration 1995, vol. II, The Hague, The Netherlands.

Menia, Z.N., 2001. Etude numérique et expérimentale de l'aéraulique dans un véhicule frigorifique. Génie des Procédés, INAPG, Paris.

Menter, F.R., 1997. Eddy viscosity transport equations and their relation to the k-epsilon model. Journal of Fluids Engineering-Transactions of the ASME 119 (4), 876–884.

Moureh, J., Menia, N., Flick, D., 2002. Numerical and experimental study of airflow in a typical refrigerated truck configuration loaded with pallets. Computer and Electronics in Agriculture 34, 25–42.

Moureh, J., Flick, D., 2003. Wall air-jet characteristics and airflow patterns within a slot ventilated enclosure. Internal Journal of Thermal Science 42, 703–711.

Moureh, J., Flick, D., 2005. Airflow characteristics within a slot-ventilated enclosure. International Journal of Heat and Fluid Flow 26, 12–24.

Nady, A., Saïd, M., Shaw, C.Y., Zhang Jianshung, S., Christianson Leslie, L., 1995. Computation of room air distribution. ASHRAE Transactions: Symposia 101, 1065–1077.

Nallasamy, M., 1987. Turbulence models and their applications to the prediction of internal flows: a review. Computers and Fluids 15 (2), 151–194.

Nielsen, P.V., Restivo, A., Whitelaw, J.H., 1978. The velocity characteristics of ventilated rooms. Journal of Fluids Engineering 100, 291–298.

Risso, F., Fabre, J., 1997. Diffusive turbulence in a confined jet experiment. Journal of Fluid Mechanics 337, 233–261.

Sharp, A., Irving, A., 1991. Air Distribution in Fantainers Stowed with Onions. CSIRO, Australia.

Timmons, M.B., Albright, L.D., Furry, R.B., Torrance, K.E., 1980. Experimental and numerical study of air movement in slot-ventilated enclosures. Transaction of the ASHRAE 86 (1).

Wang, H.W., Touber, S., 1988. Simple non-steady state modelling of a refrigerated room accounting for air flow and temperature distribution. I.I.F – I.I.R. – Commissions B1, B2, C2, D1, D2/3, 1, Wageningen, the Netherlands.

Wilcox, D.C., 1994. Turbulence Modeling for C.F.D. DCW Industries, Inc., La cañada, California.

Yu, H., Hoff, S.J., 1999. Airflow pattern similarity criteria for ceiling slot-ventilated agricultural enclosures under isothermal conditions. Transactions of the ASAE 42 (2), 459–469.

Yu, H., Liao, C.M., Liang, H.M., 2003. Scale model study of airflow performance in a ceiling slot-ventilated enclosure: isothermal condition. Building and Environment 38, 1271–1279.

Zhang, G., Morsing, S., Bjerg, B., Svidt, K., 2000. A study on the characteristics of airflow in a full scale room with a slot wall inlet, beneath the ceiling. In: ROOMVENT'2000, International Conference on Air Distribution in Rooms, Reading, UK.